

Combined NAH and Beamforming Using the Same Microphone Array

Jørgen Hald, Brüel & Kjær, Nærum, Denmark

This article deals with the problem of how to design a microphone array that performs well for measurements using both Nearfield Acoustical Holography (NAH) and Beamforming (BF), as well as how to perform NAH processing on irregular array measurements. NAH typically provides calibrated sound intensity maps, while BF provides unscaled maps. The article also describes a method to perform sound intensity scaling of the BF maps in such a way that area-integration provides a good estimate of the sub-area sound power. Results from a set of loudspeaker measurements are presented.

Figure 1 shows a rough comparison of the resolutions on the source plane, R_{BF} and R_{NAH} , that can be obtained with BF and NAH, respectively. The resolution is here defined as the smallest distance between two incoherent monopoles of equal strength on the source plane that allows them to be separated in a source map produced with the method in consideration. For BF the near-axial resolution is roughly

$$R_{BF} = 1.22 \frac{L}{D} \lambda \quad (1)$$

where L is the measurement distance, D is the array diameter and λ is the wavelength (also see Reference 1 and the Appendix). Beamforming basically performs a directional resolution of the source distribution, which explains that the resolution is proportional with the measurement distance L . Since typically the focusing capabilities of Beamforming require that all array microphones be exposed almost equally to any monopole on the source plane, the measurement distance is usually required to be not smaller than the array diameter. As a consequence, the resolution is limited to around one wavelength, which is poor at low frequencies. For NAH the resolution R_{NAH} is approximately half a wavelength at high frequencies, but at low frequencies it is never worse than approximately the measurement distance L , which can be as small as the spacing in the regular grid of measurement points.² This superior low-frequency resolution is obtained because NAH can measure very close using a regular grid, and because it has the capability of reconstructing the sound field on the source surface, including some of the evanescent waves that decay exponentially away from the source. Thus, in many cases NAH is needed at low frequencies to obtain an acceptable resolution. At high frequencies the difference is much smaller, and often an acceptable resolution can be obtained with BF, which requires far fewer measurement positions than NAH.

However, NAH requires a measurement grid with less than half wavelength spacing, and the measurement area must cover the main radiating regions to avoid windowing effects. These requirements make the method impractical at higher frequencies because too many measurement points are required. To get a comparable evaluation of the number of measurement points needed for BF, notice that usually the smallest possible measurement distance $L \approx D$ is applied to get optimal spatial resolution. With that measurement distance the mapping area within a 30° angle from the array axis is slightly larger than the array area. A large array area is therefore important to obtain a large mapping area. Fortunately, good suppression of ghost images (low sidelobe level) can be achieved in BF even when the average microphone spacing is much larger than the wavelength by the use of irregular array geometries. Thus, with a given number of microphones, BF can map a much larger area than NAH, because NAH requires less than half wavelength

spacing between measurement points to build a complete local sound field model. This often makes BF the only feasible solution at high frequencies.

A combined measurement technique using NAH at low frequencies and Beamforming at high frequencies therefore seems to provide the better of two worlds. However, traditional NAH requires a regular grid array that completely covers the sound source, while BF provides optimal high-frequency performance with an irregular array that can be smaller than the sound source. A need for repeated change between two different arrays would not be practical, but fortunately the new SONAH technique (Statistically Optimal NAH) for NAH calculations can operate with irregular arrays, and it also allows measurement with arrays smaller than the source without severe spatial windowing effects.³

The principle of the combined measurement technique is illustrated in Figure 2, using a new so-called *Sector Wheel Array* design, which will be explained further in the following section. Based on two recordings taken with the same array at two different distances (a nearfield SONAH measurement and a BF measurement at an intermediate distance), a high-resolution source map can be obtained over a very wide frequency range. The measurement distance shown for Beamforming is very small – a bit larger than half the array diameter. Simulations and practical measurements (to be described) show that with the irregular Sector Wheel Array of Figure 2 having rather uniform element density, the BF processing works well down to that distance.

Array Designs for Combined Measurement Technique

Considering first the Beamforming application, it is well known that irregular arrays provide potentially superior performance in terms of low side-lobe level over a very wide frequency band, i.e. up to frequencies where the average microphone spacing is much larger than half a wavelength.¹ The best performance is typically achieved if the set of two-dimensional spatial sampling intervals is non-redundant, i.e. the spacing vectors between all pairs of microphones are all different. In References 1 and 4 an optimization technique was introduced to adjust the microphone positions in such a way that the Maximum Side-lobe Level (MSL) is minimized over a chosen frequency range. The MSL is here defined on the basis of the so-called Array Pattern, i.e. in connection with a delay-and-sum BF method focused at infinite distance (see the Appendix and Reference 1). Since typically the MSL has many local minima when seen as a function of the design variables, an iterative optimization algorithm will usually stop at a local minimum close to the starting point. Many starting points are therefore needed to find a “good solution.” Such starting points can be generated using random number generators to ‘scan’ a certain “space of geometries.”

In References 1 and 4 the optimized array geometries were typically *Spoke Wheel Arrays* consisting of an odd number of identical line arrays arranged as spokes in a wheel (Figure 3). An odd number of spokes is used to avoid redundant spatial 2D sampling intervals. The optimization for low MSL ensures good suppression of ghost images over a wide frequency range, when the array is used at sufficiently long measurement distances, typically down to distances equal to the array diameter. If the distance becomes much smaller, the rather non-uniform density of the microphones across the Spoke Wheel Array area begin to have the effect that different points on the source plane

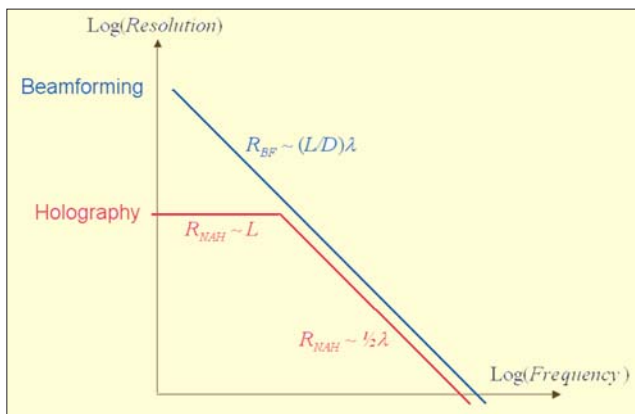


Figure 1. Resolution of Holography (NAH) and Beamforming (BF).

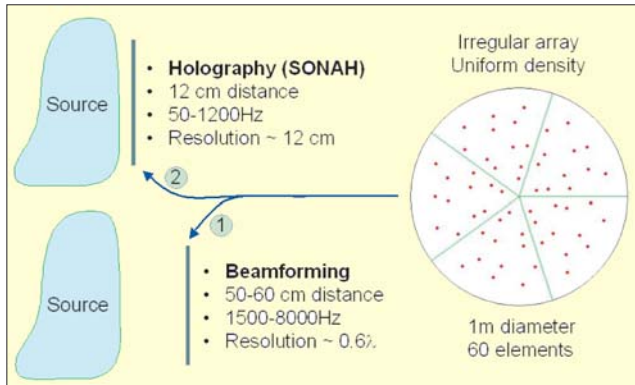


Figure 2. Principle of the combined SONAH and Beamforming technique based on two measurements with the same array.

will get very different exposure from the array. In that case, a more uniform density might be better, and numerical simulations have confirmed that hypothesis – specifically for the Sector Wheel Arrays. When the same array must also be used for nearfield holography measurements at very small distances, a more uniform density is even more necessary. This will be treated in more detail subsequently.

Various irregular array designs have been published that exhibit a more uniform density of microphones over the array area and still maintain low side-lobe levels over a wide frequency band, for example the spiral array and the packed Logarithmic Spiral Array.^{5,6} These arrays, however, lack the rotational symmetry of the Wheel Array, which allows a modular construction and can be exploited to reduce the number of geometric variables in a numerical optimization to minimize the MSL. Therefore, the Sector Wheel Array geometry was developed. Figure 4 shows a Packed Logarithmic Spiral array with 60 elements, a Sector Wheel Array with 60 elements and a Sector Wheel Array with 84 elements. For all three arrays the diameter is approximately 1 meter. The Sector Wheel Arrays maintain the rotational symmetry of the Spoke Wheel Arrays, but angularly limited sectors replace the small line arrays of the wheel. Each one of the identical sectors contains 12 elements in an irregular pattern, optimized to minimize the MSL of the array.

Figure 5 shows the MSL as a function of frequency for the three array geometries of Figure 4 and the Spoke Wheel of Figure 3, assuming focusing of the array to be within 30° from the array axis. If free focusing is required (i.e. up to 90° from the array axis), then the numbers on the frequency axis have to be multiplied by a factor of 0.75.¹ The 84-element array clearly has very low side-lobe levels at frequencies below approximately 2000 Hz, which would be 1500 Hz for the free focusing angle. With the array very close to the noise source, as required for holography processing, free focusing angle has to be considered, because waves will be incident from all sides. The 1500 Hz limit turns out to be just a little bit below the fre-

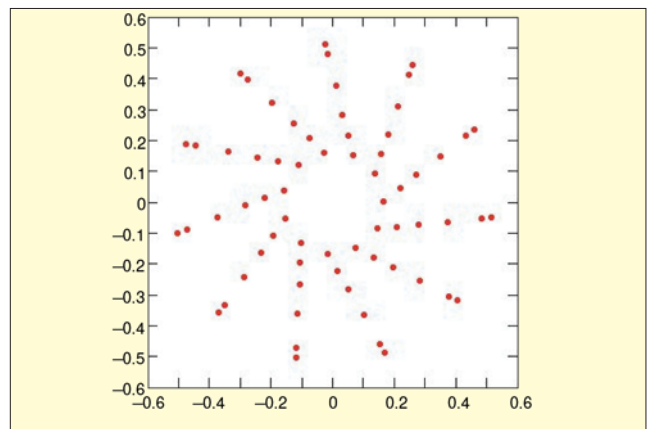


Figure 3. Typical Spoke Wheel Array geometry with 66 microphones optimized for Beamforming application.

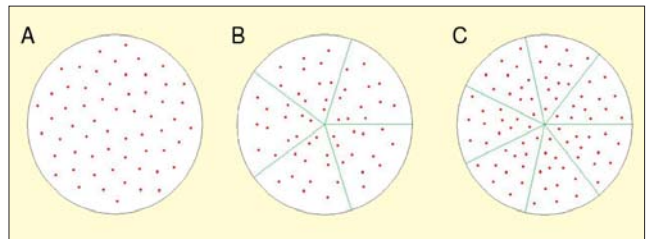


Figure 4. Three different irregular array geometries with uniform element density. The enclosing circle around all three arrays has a diameter of 1.2 m, so the array diameters are all around 1 meter. A – Packed Log. Spiral (60 microphones), B – Sector Wheel (60), C – Sector Wheel (84).

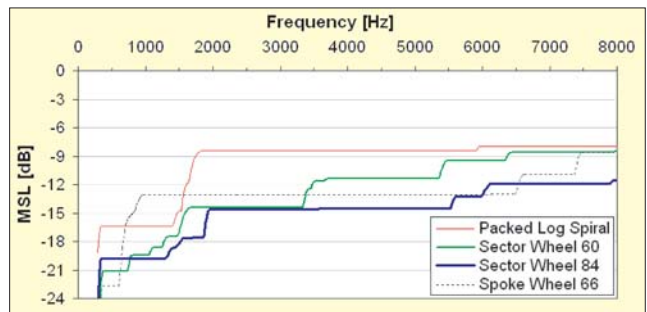


Figure 5. Maximum Side-lobe Level (MSL) for the three uniform array geometries of Figure 4 and the Spoke Wheel of Figure 3. The focusing of the array is here restricted to be within 30° from the array axis.

quency, where the average spacing between the elements of the array is half a wavelength. The average element spacing is approximately 10 cm.

Optimization of the Sector Wheel Array geometries in Figure 4 has been performed by adjusting (using a MiniMax optimization program) the coordinates of the elements in a single sector in such a way that the maximum MSL is minimized over the frequency range of interest. In this process a penalty was put on the MSL up to 1500 Hz for the 84-element array and up to 1200 Hz for the 60-element array. This turned out to help maintain the uniform element density and therefore the possibility of using the array for holography at frequencies with less than half wavelength average spacing.

These arrays with 1 m diameter have been designed for BF application in the frequency range from around 1000 Hz and up to 8000 Hz. Here, the Packed Log Spiral has the highest MSL, which is not surprising since it has not been numerically optimized for minimum MSL. As expected, the 84-channel Sector Wheel has the lowest MSL, since it has been optimized and uses the largest number of elements. The Spoke Wheel array is a bit better than the corresponding 60-element Sector Wheel over the BF frequency range, but the Sector Wheel is significantly better over a rather wide range of low frequencies, where it applies for SONAH.

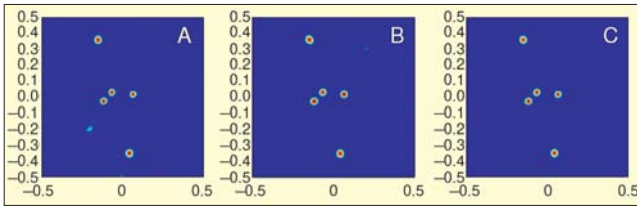


Figure 6. Simulated measurements on 5 monopoles at 8 kHz and at 60 cm measurement distance with the three array designs shown in Figure 4. The displayed range is in any case 10 dB. A – Packed Log. Spiral (60 microphones), B – Sector Wheel (60), C – Sector Wheel (84).

Simulation of Beamforming Measurements at a Small Source Distance. Some simulated measurements were performed to investigate how well the three arrays would perform with BF from a measurement distance of 0.6 m, i.e. a bit more than half the array diameter. The results are shown in Figure 6 for the case of five uncorrelated monopoles of equal strength at 8000 Hz. The Beamforming calculations have been performed using the cross-spectral algorithm with exclusion of auto-spectra,¹ focused on the source plane at a 0.6 m distance. Compared to Figure 5, the Auto-spectral exclusion reduces the MSL by approximately 1 dB at 8000 Hz for the 84-element Sector Wheel and by approximately 0.5 dB for the three other arrays. For all three plots in Figure 6 the displayed dynamic range is 10 dB, and as expected from Figure 5, the two 60-element arrays have very comparable performance at 8 kHz with a small advantage to the Sector Wheel Array. The 84-element Sector Wheel Array has 3 dB lower side-lobe level at 8 kHz, and therefore there are no visible ghost images in Figure 6. The MSL values are seen to be slightly higher at the very short measurement distance than for the infinite focus distance represented in Figure 5 – typically around 2 dB higher. The 8 kHz data presented in Figure 6 are not entirely representative for the relative performance of the three arrays over the full frequency range. If we look instead at 3 kHz, then according to Figure 4 the 60-element Sector Wheel Array has an approximately 6 dB lower side-lobe level than the 60-element Packed Logarithmic Spiral.

The following consideration illustrates the advantage of Beamforming over NAH for source location at high frequencies. If the maps in Figure 6 would have been produced with traditional NAH, then a measurement grid with dimensions around 1.2×1.2 m should have been used with a grid spacing around 2 cm, leading to approximately 3600 measurement positions!

Numerical Simulations to Clarify the Suitability of the Arrays for Holography. Another series of simulations were performed to investigate the frequency ranges over which the three arrays of Figure 4 and the Wheel Array of Figure 3 are suited for SONAH measurements. In SONAH (and other types of NAH) a complete reconstruction of the entire nearfield is attempted over a 3D region around the measurement area. This is possible only if the spatial samples of the sound field taken by the array microphones allow at least a complete reconstruction of the pressure field over the area covered by the array. So from the available spatial samples it must be possible to reconstruct (interpolate) the sound pressure across the measurement area. This can be done by the SONAH algorithm.

The problem of reconstructing a (2D) band-limited signal from irregular samples has been treated quite extensively in the literature.⁷ In order that the reconstruction be performed in a numerically stable way, it is necessary that the distribution of the sampling (measurement) points exhibit some degree of uniform density across the sampling area. Such a criterion was used in the design of the Sector Wheel Arrays.

A set of eight monopole point sources at 30 cm distance from the array was used for the numerical simulations. All point sources were inside an area of the same size as the arrays. For each frequency and each point source, the complex pressure was calculated at the array microphone positions, and SONAH was then applied to calculate the sound pressure over a dense grid of points inside the measurement area in the measurement

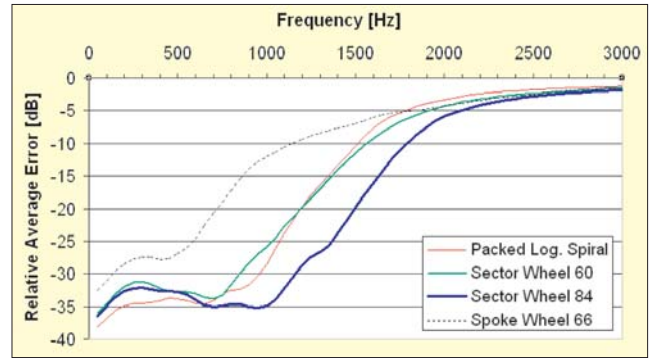


Figure 7. Comparison of Relative Average Interpolation Error for the three arrays in Figure 4 and the Wheel Array of Figure 3. The error is averaged over a set of monopole point sources at 30 cm distance.

plane. A 40 dB dynamic range was used.³ The interpolated pressure from each monopole was then compared with the known pressure from the same monopole, and the Relative Average Error was estimated at each frequency as the ratio between a sum of squared errors and a corresponding sum of squared true pressure values. The summation was in both cases over all interpolation points and all sources.

Figure 7 gives a comparison of the Relative Average Interpolation Errors obtained with the four different arrays. Clearly, the 84-element optimized Sector Wheel Array can represent the sound field over the array area up to around the previously mentioned 1500 Hz, while the 60-element Sector Wheel Array provides acceptable accuracy only up to around 1200 Hz. This actually means that the two Sector Wheel Arrays apply over the same frequency ranges as regular arrays with the same average element spacing. The 60-element Packed Logarithmic Spiral is seen to perform much like the 60-element Sector Wheel Array in connection with SONAH calculations. But as expected, the 66-element Spoke Wheel Array performs much more poorly than the three arrays with more uniform element density. The acceptable interpolation accuracy (20 dB suppression of errors) is achieved only up to approximately 700 Hz. If the monopole sources had been positioned nearer the array, this upper frequency would have been even lower.

Intensity Scaling of Beamformer Output

When combining low-frequency results obtained with SONAH and high-frequency results obtained with Beamforming, it is desirable to scale the results in the same way. However this is not straightforward, as will be apparent from the following description of the basic output from SONAH and BF.

Based on the measured pressure data, SONAH builds a sound field model valid within a 3D region around the array, and using that model it is possible to map any sound field parameter. Typically the sound intensity normal to the array plane is calculated to get the information about source location and strength. Since the measurement is taken very near the sources, the energy radiated in any direction within a 2π solid angle will be captured and included with the sound intensity and sound power estimates.

Beamforming, on the other hand, is based on a measurement taken at some intermediate distance from the sources where only a fraction of the 2π solid angle is covered by the array. Rather than estimating sound field parameters for the source region, a directional filtering is performed on the sound field incident towards the array. As a result, only the relative contributions to the sound pressure at the array position from different directions is obtained. Reference 8 describes a scaling of the output that allows the contribution at the array position from specific source areas to be read directly from the Beamformed maps. Of course this is meaningful only if the pressure distribution across the array area from the various partial sources is rather constant, which will be true if the array covers a relatively small solid angle as seen from the sources.

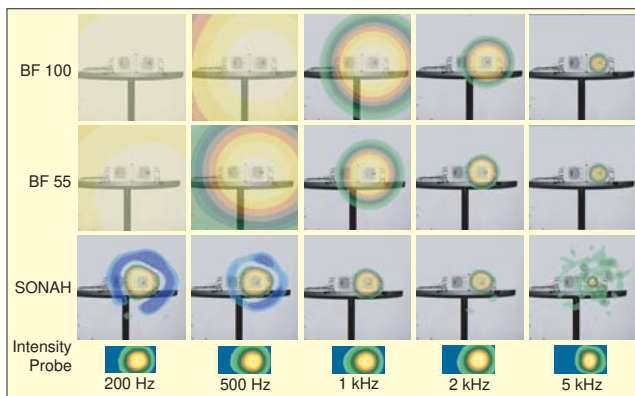


Figure 8. 1/3-octave sound intensity maps for the measurements with only the rightmost speaker excited. The four rows represent Beamforming from 100 and 55 cm distance, SONAH from 12 cm distance and measurement with a sound intensity probe at 7 cm distance. Dynamic range is in any case 15 dB.

However, in the context of this article we wish to take BF measurements as close as possible to the source area in order to obtain the best possible spatial resolution. As a consequence, the radiation into a rather large fraction of the 2π solid angle is measured, so we should be in a better position to get information about the sound power radiated through the source plane. Wanting to scale the Beamformer output such that the scaled map represents in some way the source signal strength, it seems logical to scale as active sound intensity because that quantity represents the radiation towards the array and into the farfield region. Nearfield pressure contains evanescent components that are not picked up by the array.

The Appendix describes the derivation of a method to scale the output from a delay-and-sum Beamformer in such a way that area integration of the scaled output provides a good estimate of the sub-area sound power, leading to the term “Sound Intensity Scaling.” The derivation is performed by looking at a single monopole point source in the farfield region, and assuming that the array provides good angular resolution, i.e. assuming that the mainlobe covers only a small solid angle. An evaluation is given then of the errors introduced by the farfield assumption and the assumption of a narrow mainlobe, done both for delay-and-sum processing and for the Cross-spectral algorithm with exclusion of Auto-spectra. The main conclusions are for the 60-element Sector Wheel Array of Figure 4 and for frequencies above 1200 Hz:

1. The error is less than 0.4 dB when using a measurement distance not smaller than the array diameter.
2. At smaller measurement distances the error increases, but it does not exceed approximately 0.6 dB when the distance is larger than 0.6 times the array diameter.

In the Appendix it is argued that if the scaling works for a single omni-directional source, then it holds also for a set of incoherent monopole sources in the same plane. If sources are partially coherent and/or if single sources are not omni-directional, then because of the limited angular coverage of the array, accurate sound power estimation cannot possibly be obtained. Fortunately, many real-world sound sources tend to have low spatial coherence in the frequency range where Beamforming will be used in the combined NAH/BF method.

The derivation of the scaling is based on matching the area-integrated map with the known sound power for a monopole sound source. In the derivation, area integration was performed over only the hot spot corresponding to the mainlobe of the beamformer. At high frequencies many sidelobes will typically be within the mapping area, and it turns out that area-integration over a large number of sidelobes will typically contribute significantly to the sound power. This effect will be limited in practice by the use of a finite dynamic range during the area integration, typically around 10 dB. A frequency dependent adjustment of the integration area to match the resolution is not practical. The efficiency of limiting the dynamic range in

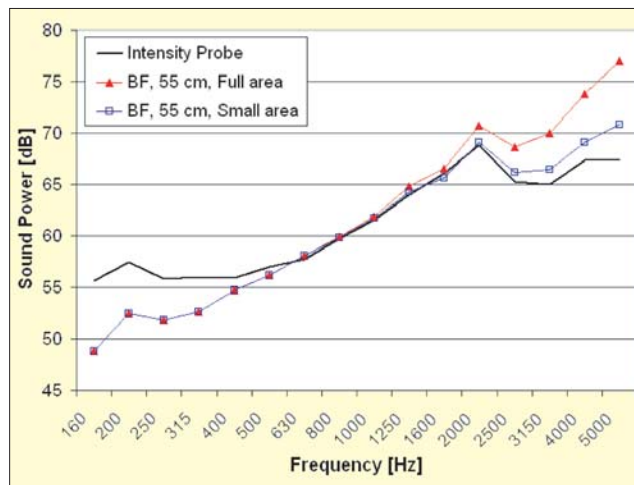


Figure 9. 1/3-octave sound power spectra for the single speaker measurement. The intensity probe map has been integrated over the entire mapping area shown in Figure 8. The Beamforming measurement taken at 55 cm distance has been integrated over the full mapping area and over only the mainlobe area.

the area integration will be described in a paper to be presented at the SAE Noise and Vibration Conference, 2005.

The measurement results to be presented in the following section will show the influence of the measurement distance, of the size of the power integration area and of the presence of more than a single source. Also, the sound power estimates will be compared with sound power data obtained from sound intensity maps measured with a sound intensity probe.

Measurements

In order to test the performance of the 60-element Sector Wheel Array of Figure 4, measurements were taken at 12 cm distance from two small loudspeakers for SONAH processing, and at 55 cm and 100 cm distance for BF processing. The microphones used in the array were B&K Type 4935. At all three distances, measurements were taken with coherent and incoherent white noise excitation of the two speakers and also with only one speaker excited. For each of these three excitations, a scan was performed approximately 7 cm in front of the two loudspeakers with a B&K sound intensity probe Type 3599. The two speakers were identical small PC units with drivers of diameter 7 cm and they were mounted with 17 cm between the centers of the drivers. The arrangement of the speakers can be seen in some of the contour plots in Figure 8. The Beamforming processing was performed with the Cross-spectral algorithm with exclusion of Auto-spectra.¹

Figure 8 shows resulting 1/3-octave intensity maps for the measurements with only the rightmost speaker excited. The four rows of contour plots represent Beamforming from 100 and 55 cm distance, SONAH from 12 cm distance and measurement with the sound intensity probe at 7 cm distance, respectively. For the first three rows representing Beamforming and SONAH results, the sound intensity has been estimated in the source plane over an area of approximate size 80 cm \times 80 cm, while the last row shows the sound intensity measured 7 cm from the plane of the speakers over an area 36 cm \times 21 cm. All plots show a 15 dB dynamic range from the maximum level, with 1.5 dB steps between the colors. Yellow/orange/green colors represent outwards intensity and blue colors represent inwards intensity. The absolute levels will be presented subsequently through area integrated sound power data.

The resolution obtained with Beamforming and SONAH is in good agreement with the expectations of Figure 1. The bend on the resolution curve for SONAH is in this case at approximately 1500 Hz, being determined by $1/2\lambda = L$ where L is the measurement distance and λ is wavelength. Clearly, at low frequencies the Beamforming resolution is very poor, while above approximately 1.5 kHz it is approximately as good as that obtained with the sound intensity probe. SONAH provides good

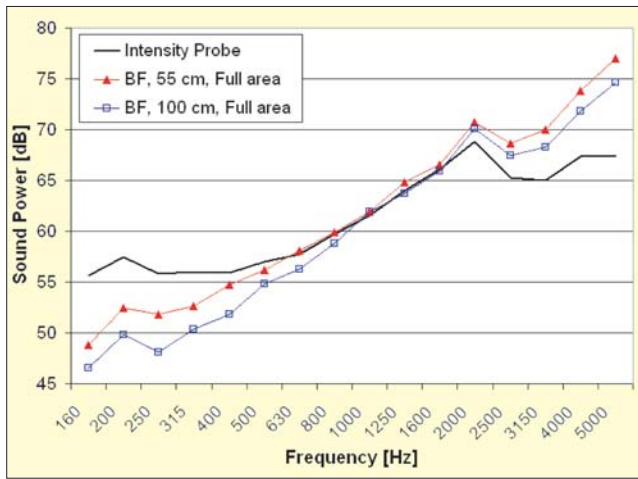


Figure 10. 1/3-octave sound power spectra for the single speaker measurement. Again the intensity probe result is included. But now the results from Beamforming measurements at 55 cm and at 100 cm distance are included. For both of these, the sound power integration covers the entire mapping area.

resolution over the entire frequency range, but above approximately 1200 Hz, the average spacing of the microphone grid is too large to reconstruct the sound pressure variation across the measurement area. As a result, distortions will slowly appear as frequency increases. More evidently, the level will be underestimated as can be seen in the sound power spectra of Figures 11 and 12. The combined method using SONAH up to 1250 Hz and Beamforming at higher frequencies provides good resolution and sound power estimates at all frequencies, as shown in Figures 11 and 12. So two recordings taken with the Sector Wheel array at two different distances can provide the information obtained with a time consuming scan with an intensity probe (104 positions for the small plots in Figure 8), and additionally many other types of analyses can be performed based on the same data, such as transient analysis of radiation phenomena.

As mentioned previously, the sound intensity scaling of the output from Beamforming is defined in such a way that area integration over the mainlobe area will provide a good estimate of the sound power from a monopole point source. Figure 9 depicts the 1/3-octave sound power spectra for the single speaker obtained from the scan with the sound intensity probe and from the Beamforming measurement at 55 cm distance. The intensity probe measurement has been integrated over the full measurement area shown in Figure 8. Two curves are shown for the sound power obtained with the Beamforming measurement – one obtained by integration over the full mapping area and another obtained by integration over a small rectangular area with x - and y -dimensions equal to the mainlobe diameter and centered at the known point source position. The radius of the mainlobe is $1.22\lambda L/D$, where λ and L are wavelength and measurement distance (55 cm) as defined above, and D is the array diameter of approximately 1 m (see Eq. A15 in the Appendix). At low frequencies the mainlobe is larger than the entire mapping area of 0.8×0.8 m, and therefore the two Beamforming spectra are identical. Here, the sound power is underestimated, because the power outside the mapping area is not included, and also the assumptions made for the sound intensity scaling fail to hold, see the Appendix. At high frequencies the power estimated by Beamforming is too high, even when the integration covers only the mainlobe area. This is mainly because the loudspeaker is no longer omni-directional as assumed in the scaling, but concentrates the radiation in the axial direction, towards the array. At 5 kHz the diameter of the driver unit is approximately one wavelength. Another reason for the overestimation could be the tendency of the intensity scaling to overestimate when the measurement distance is very small (see Figure A3). Looking at the sound power obtained by integration over the entire mapping area, it is even higher at

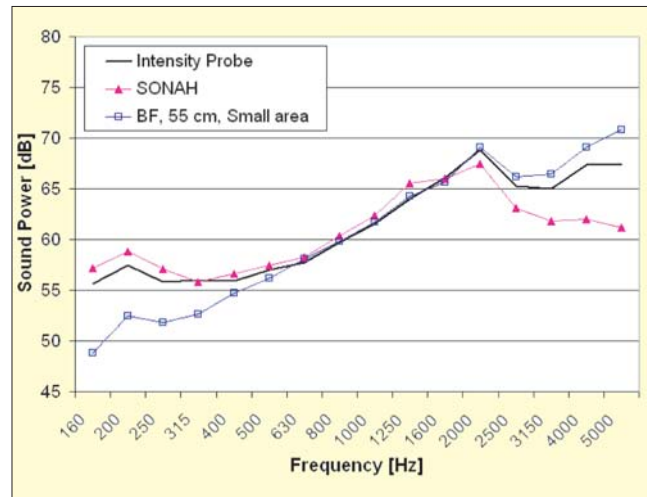


Figure 11. 1/3-octave sound power spectra for the single speaker measurement. The results obtained with Intensity Probe, SONAH and Beamforming are compared.

the high frequencies. The reason is that sidelobes (ghost images) contribute significantly when the integration area is much larger than the mainlobe area, even when the array has good sidelobe suppression as the present Sector Wheel array.

Figure 10 shows results similar to those of Figure 9, but instead of focusing on the influence of the size of the power integration area, the influence of the measurement distance is now investigated. For both of the two Beamforming measurements taken at different distances, the power integration has been performed over the entire mapping area. At low frequencies, the strongest underestimation results from the measurement taken at the longest distance, because the resolution is worse and consequently a larger part of the power falls outside the mapping area. At high frequencies the measurement at 55 cm distance produces the strongest overestimation. There are several reasons. One is that the sidelobes become a bit stronger at measurement distances smaller than the array diameter. Another is the better resolution – a narrower mainlobe means that the ratio between the sidelobe-area and the mainlobe-area increases significantly. Finally, the scaling tends to overestimate the sound power when used with measurements taken at very small distances, as can be seen in Figure A3.

Figure 11 shows the 1/3-octave sound power spectra for the single loudspeaker obtained with an intensity probe, SONAH and Beamforming. The BF measurement at 55 cm distance has been chosen, and for that measurement the sound power integration has been performed only over the small area of the same size as the mainlobe. Above 500 Hz this leads to a good estimate of the sound power, apart from the previously discussed overestimation at the highest frequencies. But the spatial resolution is poor below around 1 kHz. SONAH provides good sound power estimates up to around 1.6 kHz, apart from a small overestimation, which could be due to the measurement area used with the sound intensity probe being a bit too small. However, above 1.6 kHz the sound power is increasingly underestimated with SONAH.

As expected, the results with equal but incoherent excitation of the two speakers are very similar to the results with only one loudspeaker excited. The sound power spectra all increase by approximately 3 dB over the major part of the frequency range, but the differences between the spectra remain unchanged. Therefore no results are shown here.

Equal but coherent in-phase excitation of the two loudspeakers will, on the other hand, cause the radiation to deviate more from being omni-directional, which violates the assumptions on which the intensity scaling of Beamformer maps are based. Figure 12 depicts the 1/3-octave sound power spectra obtained using the intensity probe, SONAH and Beamforming with identical excitation of the two speakers. The SONAH spectrum follows the intensity probe spectrum in much the same way as

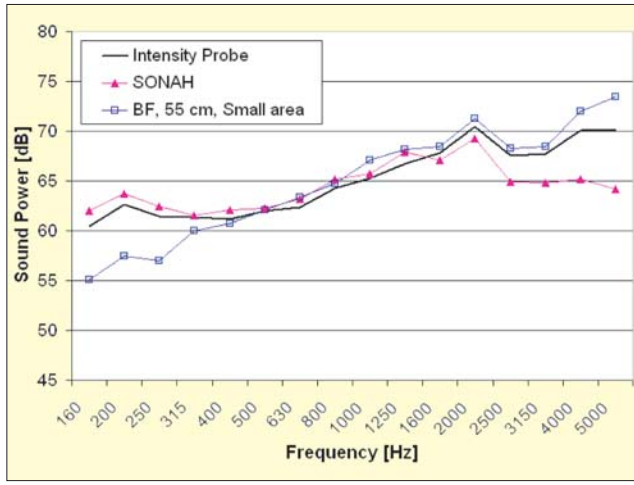



Figure 12.1/3-octave sound power spectra for the case of the two speakers being excited with the same white noise signal. Results obtained with Intensity Probe, SONAH and Beamforming are compared.

for the case of only a single speaker being excited. But the sound power obtained from the scaled Beamformer map shows additional deviation in the frequency range from 1 kHz to 2 kHz. In that frequency range the distance between the two speakers is between half a wavelength and one wavelength, which will focus the radiation in the axial direction. But the deviation remains within approximately 2 dB from the power spectrum obtained with the sound intensity probe.

Conclusions

A new combined array measurement technique has been presented that allows NAH and Beamforming to be performed with the same microphone array. This combination can provide high-resolution noise source location over a very broad frequency range based on two recordings with the array at two different distances from the source. The functionality is all supported in Pulse Version 9.0 from Brüel & Kjær.

References

- Christensen, J. J. and Hald, J. "Beamforming." Brüel & Kjær Technical Review, No. 1, 2004.
- Williams, E. G. "Fourier Acoustics – Sound Radiation and Nearfield Acoustical Holography." Academic Press, 1999.
- Hald, J. "Patch Nearfield Acoustical Holography using a New Statistically Optimal Method." Proceedings of Inter-Noise 2003.
- Hald, J. and Christensen, J. J. "A Class of Optimal Broadband Phased Array Geometries designed for Easy Construction." Proceedings of Inter-Noise 2002.
- Nordborg, A., Wedemann, J. and Willenbrink, L. "Optimum Array Microphone Configuration." Proceedings of Inter-Noise 2000.
- Boeringer, D. W. "Phased Array including a Logarithmic Lattice of Uniformly Spaced Radiating and Receiving Elements." United States Patent US 6,433,754 B1.
- Unser, M. "Sampling – 50 Years After Shannon." Proceedings of the IEEE, Vol. 88, No. 4, April 2000.
- Oerlemans, S. and Sijtsma, P. "Determination of Absolute Levels from Phased Array Measurements Using Spatial Source Coherence." AIAA 2002-2464.
- Johnson, D. H. and Dudgeon, D. E., *Array Signal Processing: Concepts and Techniques*. Prentice Hall, New Jersey, 1993. 

The author can be contacted at: jhald@bksv.com.

Sound Intensity Scaling of BF Output

Introduction to Delay-and-Sum Beamforming with Infinite Focus Distance. As illustrated in Figure A1, we consider a planar array of M microphones at locations \mathbf{r}_m ($m = 1, 2, \dots, M$) in the xy -plane of our coordinate system. When such an array is applied for delay-and-sum Beamforming, the measured pressure signals p_m are individually weighted and delayed,

and then all signals are summed:⁹

$$b(\boldsymbol{\kappa}, t) = \frac{1}{M} \sum_{m=1}^M w_m \cdot p_m(t - \Delta_m(\boldsymbol{\kappa})) \quad (\text{A1})$$

The individual time delays Δ_m are chosen with the aim of achieving selective directional sensitivity in a specific direction, characterized here by a unit vector $\boldsymbol{\kappa}$. This objective is met by adjusting the time delays in such a way that signals associated with a plane wave, incident from the direction $\boldsymbol{\kappa}$, will be aligned in time before they are summed. Geometrical considerations (see Figure A1) show that this can be obtained by choosing

$$\Delta_m = \frac{\boldsymbol{\kappa} \cdot \mathbf{r}_m}{c} \quad (\text{A2})$$

where c is the propagation speed of sound. Signals arriving from other farfield directions will not be aligned before the summation, and therefore they will not coherently add up. The weights w_m of the microphone signals are all set to one here.

The frequency domain version of Eq. A1 for the delay-and-sum beamformer output with the weights equal to one is

$$B(\boldsymbol{\kappa}, \omega) = \frac{1}{M} \sum_{m=1}^M P_m(\omega) \cdot e^{-j\omega\Delta_m(\boldsymbol{\kappa})} = \frac{1}{M} \sum_{m=1}^M P_m(\omega) \cdot e^{j\mathbf{k} \cdot \mathbf{r}_m} \quad (\text{A3})$$

Here, ω is the temporal angular frequency, $\mathbf{k} \equiv -k\boldsymbol{\kappa}$ is the wave number vector of a plane wave incident from the direction $\boldsymbol{\kappa}$ in which the array is focused (see Figure A1) and $\mathbf{k} = \omega/c$ is the wave number. In Eq. A3 an implicit time factor equal to $e^{j\omega t}$ is assumed.

Through our choice of time delays $\Delta_m(\boldsymbol{\kappa})$, or equivalently of the 'preferred' wave number vector $\mathbf{k} \equiv -k\boldsymbol{\kappa}$, we have 'tuned' the beamformer on the farfield direction $\boldsymbol{\kappa}$. Ideally we would like to measure only signals arriving from that direction, in order to get a perfect localization of the sound source. To investigate how much 'leakage' we will get from plane waves incident from other directions, we assume now a plane wave incident with a wave number vector \mathbf{k}_0 different from the preferred $\mathbf{k} \equiv -k\boldsymbol{\kappa}$. The pressure measured by the microphones will then ideally be

$$P_m(\omega) = P_0 e^{-j\mathbf{k}_0 \cdot \mathbf{r}_m} \quad (\text{A4})$$

which according to Eq. A3 will give the following output from the beamformer

$$B(\boldsymbol{\kappa}, \omega) = \frac{P_0}{M} \sum_{m=1}^M e^{j(\mathbf{k} - \mathbf{k}_0) \cdot \mathbf{r}_m} \equiv P_0 W(\mathbf{k} - \mathbf{k}_0) \quad (\text{A5})$$

Here, the function W

$$W(\mathbf{K}) \equiv \frac{1}{M} \sum_{m=1}^M e^{j\mathbf{K} \cdot \mathbf{r}_m} \quad (\text{A6})$$

is the so called *Array Pattern*, defined entirely by the array geometry. It has the form of a generalized spatial DFT of the weighting function, which in this case has been set equal to one at all microphone positions. Because the microphone positions \mathbf{r}_m have a z -coordinate equal to zero, the Array Pattern is independent of K_z . We shall therefore consider the Array Pattern W only in the (K_x, K_y) plane, i.e. we consider the projections of the wave number vectors onto that plane. There, W has an area with high values around the origin with a peak value equal to 1 at $(K_x, K_y) = (0, 0)$. According to Eq. A5, this peak represents the high sensitivity to plane waves coming from the direction $\boldsymbol{\kappa}$, in which the array is focused. Figure A1 contains an illustration of that peak, which is called the *mainlobe*. Other directional peaks, which are called *sidelobes*, will cause waves from such directions to leak into the measurement of the mainlobe direction $\boldsymbol{\kappa}$. The *Maximum Sidelobe Level* (MSL) is defined as the ratio between the highest sidelobe and the mainlobe for a given frequency range.

In Eq. A5 for the response to a plane wave, notice that the output is exactly equal to the amplitude P_0 of the plane wave, when the array is focused towards the direction of incidence of the plane wave, i.e. when $\mathbf{k} = \mathbf{k}_0$.

For stationary sound fields it is natural to operate with the

matrix of cross spectra between the microphones, which provides a better average representation of stationary phenomena. Exclusion of the auto-spectra offers the possibility of reducing the influence of noise in the individual measurement channels, and it turns out that it also often reduces the sidelobe level.¹ For the derivation of the sound intensity scaling we will, however, not use the Cross-spectral formulation. But the scaling holds for the Cross-spectral formulation as well, as long as it is scaled in such a way that the response to an incident plane wave is equal to the squared amplitude of the wave. The formulation in Reference 1 is scaled that way. The validity of the intensity scaling in combination with the Cross-spectral Beamformer is investigated both through simulations in this appendix and through the practical measurements.

From the literature it is known that the size and shape of the mainlobe of the array pattern is determined almost entirely by the size and overall shape of the array,^{1,9} while the sidelobes are highly affected by the actual positions of the microphones. The shape of the mainlobe is usually close to the mainlobe from a “continuous aperture” of the same shape as the array or, equivalently, a very densely populated array covering the same area. For circular array geometry, the equivalent continuous aperture has the following array pattern:

$$\bar{W}(K) = 2 \frac{J_1(\frac{1}{2}KD)}{\frac{1}{2}KD}, \quad K \equiv |\tilde{\mathbf{K}}| \quad (\text{A7})$$

where D is the diameter of the aperture (or equivalently of the array), J_1 is the Bessel function of order 1, and $\tilde{\mathbf{K}}$ is the projection of vector \mathbf{K} onto the array plane. What we have achieved here is a general approximation for the shape of the mainlobe, which is independent of the specific positioning of the microphones,

$$W(\mathbf{K}) \approx \bar{W}(|\tilde{\mathbf{K}}|) \quad \text{for} \quad |\tilde{\mathbf{K}}| \leq K_1 \quad (\text{A8})$$

Here, K_1 is the first null of the aperture array pattern, $\bar{W}(K_1) = 0$, given by

$$\frac{1}{2} K_1 D = \xi_1 \approx 3.83 \quad (\text{A9})$$

ξ_1 being the first null of the Bessel function of the first order.

Derivation of the Scaling. For the derivation we now assume a single monopole point source on the array axis at sufficiently large distance L that the amplitude and phase of the pressure is practically constant across the array area. Thus, for the array the sound field is a plane wave with amplitude P_0 incident with wave number vector $\mathbf{k}_0 = -k\hat{z}$, where \hat{z} is the unit vector in the z -direction. The sound power P_a radiated by the monopole is then

$$P_a = 4\pi L^2 \cdot I = 4\pi L^2 \cdot \frac{|P_0|^2}{2\rho c} = 2\pi L^2 \cdot \frac{|P_0|^2}{\rho c} \quad (\text{A10})$$

where I is the sound intensity at the position of the array and ρ is the density of the medium.

From Eq. A5 we get for the output from the delay-and-sum beamformer

$$B(\boldsymbol{\kappa}) = P_0 W(\mathbf{k} - \mathbf{k}_0) = P_0 W(-k\boldsymbol{\kappa} + k\hat{z}) \quad (\text{A11})$$

where the known values of the two wave number vectors have been inserted. In order to use the approximation (Eq. A8) for the mainlobe of the array pattern, we need to project the wave number vectors onto the xy -plane, which leads to

$$B(\boldsymbol{\kappa}) \approx P_0 \bar{W}(k \sin(\theta)) \quad \text{for} \quad |k \sin(\theta)| \leq K_1 \quad (\text{A12})$$

θ being the angle from the array axis (the z -axis) to the focus direction $\boldsymbol{\kappa}$.

The beamformer is now used to create a source map in the plane $z = L$. Each position on this source plane is described by its distance R to the z -axis and its azimuth angle ϕ . Assuming relatively small angles from the z -axis we can use the approximation

$$R = L \tan(\theta) \approx L \sin(\theta) \quad (\text{A13})$$

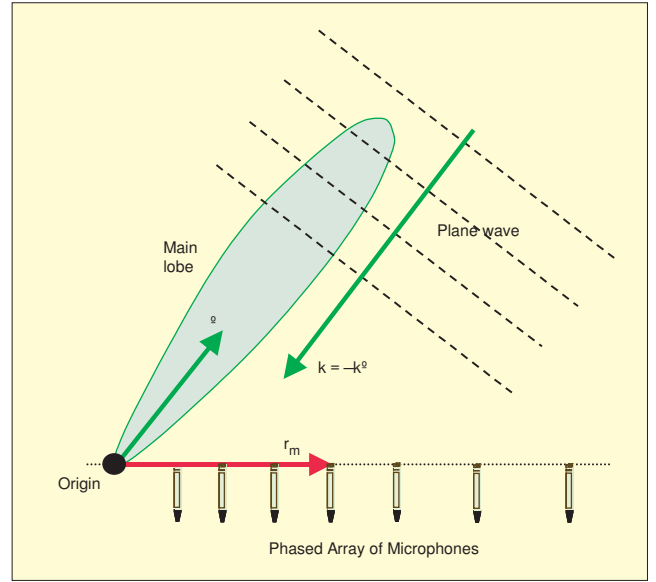


Figure A1. Illustration of a phased microphone array, a directional sensitivity represented by a mainlobe, and a plane wave incident from the direction of the mainlobe.

where θ is still the angle to the z -axis. Use of Eq. A13 in Eq. A12 leads to the following approximate expression for the ‘mainlobe’ of the beamformed map on the source plane

$$B(R, \phi) \approx P_0 \bar{W}\left(\frac{kR}{L}\right) \quad \text{for} \quad R \leq \frac{K_1 L}{k} = R_1 \quad (\text{A14})$$

By the use of Eq. A9, we get for the radius R_1 of the mainlobe on the source plane

$$R_1 \equiv \frac{K_1 L}{k} = \frac{2L}{kD} \xi_1 \approx 1.22 \frac{L\lambda}{D} \quad (\text{A15})$$

The scaling factor α needed to obtain the intensity scaled beamformer output,

$$B_I(R, \phi) = \alpha \cdot |B(R, \phi)|^2 \quad (\text{A16})$$

is now defined in such a way that the integral of $B_I(R, \phi)$ over the mainlobe equals half of the radiated sound power P_a , i.e. the power radiated into the hemisphere containing the array

$$\begin{aligned} \frac{1}{2} P_a &= \int_0^{R_1} \int_0^{2\pi} \alpha |B(R, \phi)|^2 R dR d\phi \\ &= 2\pi \alpha |P_0|^2 \int_0^{R_1} \bar{W}^2\left(\frac{kR}{L}\right) R dR \end{aligned} \quad (\text{A17})$$

Use of Eq. A7, substitution with the variable

$$u \equiv \frac{kR}{L} = \frac{kD}{2L} R \quad (\text{A18})$$

for R in Eq. A17 and application of Eq. A15 leads to

$$\begin{aligned} \frac{1}{2} P_a &= 2\pi \alpha |P_0|^2 \int_0^{\xi_1} \left[2 \frac{J_1(u)}{u} \right]^2 \left(\frac{2L}{kD} \right)^2 u du \\ &= \alpha \cdot 32\pi \left(\frac{|P_0|L}{kD} \right)^2 \cdot \Gamma \end{aligned} \quad (\text{A19})$$

with

$$\Gamma \equiv \int_0^{\xi_1} \left[\frac{J_1(u)}{u} \right]^2 u du \approx 0.419 \quad (\text{A20})$$

The scaling factor can finally be obtained through use of Eq. A10 for the sound power in Eq. A19

$$\alpha = \frac{1}{32\Gamma} \frac{(kD)^2}{\rho c} \approx \frac{2.94}{\rho c} \left(\frac{D}{\lambda} \right)^2 \quad (\text{A21})$$

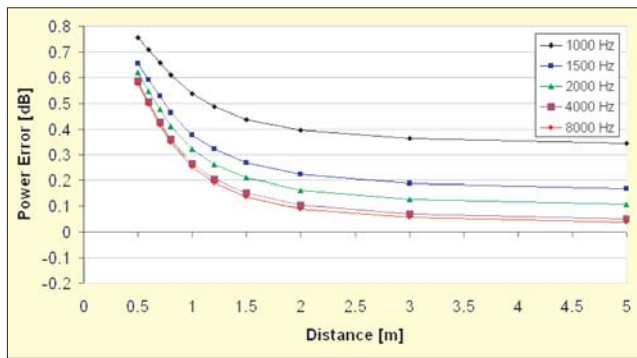


Figure A2. Difference in decibels between estimated and true Sound Power. The estimated value is from an Intensity-scaled Delay-And-Sum Beamformer. The source is a monopole on the array axis.

Clearly, the scaling factor is proportional with the square of the array diameter measured in wavelengths. This is natural, because the unscaled beamformer output $B(\hat{z})$ with the array focused towards the point source is basically independent of array geometry, but the width of the mainlobe is inversely proportional with the array diameter measured in wavelengths (see Eq. A15). To maintain the area-integrated power with increasing array diameter, the scaling factor must have the mentioned proportionality.

Evaluation of Errors. The major principle of the scaling is that area integration of the scaled output must provide a good estimate of the sub-area sound power, lending the term “Sound Intensity Scaling” to the method. The scaling is defined for a single omni-directional point source in such a way that area integration of the peak created by the mainlobe equals the known radiated power from the point source. So by this definition the total power will be within the mainlobe radius from the source position, and integration over a larger area will cause an overestimation of the sound power. One reason for choosing this definition is that only the mainlobe has a form that depends only on the array diameter and not on all microphone positions. Other choices would be somewhat arbitrary, would require integration over a larger area to get the total power and would need the scaling factor to depend on the particular set of microphone positions. But the influence of the sidelobes on the power integration is a weakness. If the mainlobe is rather narrow and sound power integration is performed over an area much larger than the size of the mainlobe on the source plane, then the level of sidelobes often present in beamforming can contribute significantly to the power integration and cause a significant overestimation of the sound power.

The scaling was derived for a single omni-directional point source on the array axis. Beyond that we have assumed the monopole to be so far away from the array that its sound field has the form of a plane wave across the array. Thus, we have assumed the source to be in the farfield region relative to the array. The second important assumption introduced in Eq. A13-14 above is that the mainlobe covers a relatively small solid angle. To investigate the effect of the latter two assumptions, a series of simulations have been performed with the 60-channel Sector Wheel Array of Figure 4 and with a single monopole point source at different distances on the array axis and operating at different frequencies. The beamforming calculation has been performed with two different beamformers:

1. A delay-and-sum beamformer focused at the finite source distance, but without any amplitude compensation.¹
2. The Cross-spectral beamformer with exclusion of Auto-spectra described in Reference 1. This method compensates for the amplitude variation across the array of the sound pressure from a monopole on the source plane.

The output has then been scaled as sound intensity through multiplication with the scaling factor α of Eq. A21, and finally the sound power has been estimated by integration over a circular area with radius equal to R_1 (ref. Eq. A15) around the array axis.

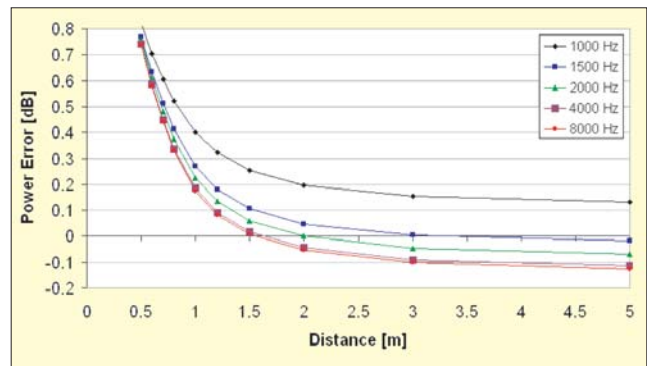


Figure A3. Difference in decibels between estimated and true Sound Power. The estimated value is from an Intensity-scaled Cross-spectral Beamformer with exclusion of Auto-spectra. The source is a monopole on the array axis.

Figure A2 shows the ratio between the estimated and the exact sound power in decibels for the case of the delay-and-sum beamformer. At 1000 Hz the mainlobe (and therefore the hot spot generated around the source position on the array axis) covers an angle of approximately 24° from the array axis. This will introduce a significant error in Eqs. (A13-14) and therefore an error in the estimated sound power, even when the source distance is relatively large. Fortunately, SONAH applies below approximately 1200 Hz for the particular array, so beamforming will be used typically only above that frequency, and here the error is quite small, provided the measurement distance is not too small. The error increases quickly for distances smaller than approximately 1 m, which is the approximate diameter of the array. Here, the assumption of the source being in the farfield region relative to the array certainly does not hold. But fortunately the error does not get worse than approximately 0.6 dB for distances down to half the array diameter. To achieve the best possible resolution it is desirable to use the array at such small measurement distances.

Figure A3 shows the difference between the estimated and the exact sound power in decibels for the case of the Cross-spectral beamformer with exclusion of Auto-spectra.¹ This algorithm is implemented in Brüel & Kjær’s stationary and quasi-stationary beamforming calculation software, and therefore it has been used for the measurements presented here. Comparison of Figures 3 and 4 show that in general the Cross-spectral algorithm produces smaller errors than the delay-and-sum algorithm, except at the very short measurement distance of 0.5 m.

It is also important to consider how the sound intensity scaling works for more realistic source distributions than a single monopole. Consider first the case of several omni-directional, but mutually incoherent point sources in the source plane. The incoherent sources will contribute independently to the Cross-spectral matrix between the microphones, i.e. the matrix will be the sum of elementary matrices related to each one of the point sources. If a Cross-spectral beamformer is used, then the (power) output will equal the sum of contributions from the elementary matrices, meaning that the incoherent partial sources contribute additively to the beamformer (power) output. Since they also contribute additively to the sound power, the conclusion is that the intensity scaling will hold for a set of incoherent monopole point sources.

When there is full or partial coherence between a set of monopole sources, the radiation from the total set of sources is no longer omni-directional. This will introduce an error that cannot be compensated – the array covers only a certain part of the 2π solid angle for which the sound power is desired. For angles not covered by the array we do not know the radiation and therefore we cannot know the sound power.